 doi:10.20944/preprints202010.0613.v1

Research on the method of gas emission prediction using improved grey RBF neural network model

Yongkang Yang[1,2*], Qiaoyi Du[1], Chenlong Wang[1], Yu Bai[1]

1 Key Laboratory of In-situ Property-improving Mining of Ministry of Education, Taiyuan University of Technology，Taiyuan，Shanxi 030024，China;

2 State Key Laboratory of Coal Resources and Safe Mining，China University of Mining & Technology(Beijing), 100083, Beijing, China.

***Corresponding author.**

Tel: +86-13203413056

Email: **yongkang8396**@163.com

Postal address: Key Laboratory of In-situ Property-improving Mining of Ministry of Education, Taiyuan University of Technology，Taiyuan，Shanxi 030024，China

Abstract: Effectively avoiding gas accident is vital to the security of mineral manufacture, and the coal mine gas accident is often caused by gas concentration overrun. The prediction accuracy of gas emission quantity in coal mine is the key to solve this problem. To maintain concentration of gas in a secure range，grey theory and neural network model increasingly diffusely used in forecasting gas emission quantity in coal mine critically. Nevertheless, the limitation of the grey neural network model is that researchers merely bonded the conventional neural network and grey theory. To enhance accuracy of prediction, a modified grey GM(1,1) and RBF neural network model is proposed combined amended grey GM(1,1) model and RBF neural network model. Then the proposed model was put into simulation experiment which is built based on Matlab software. Ultimately, conclusion of the simulation experiment verified that the modified grey GM(1,1) and RBF neural network model not only boosts the precision of prediction, but also restricts relative error in a minimum range. This showed that the modified grey GM(1,1) and RBF neural network model achieves effectiveness in precision of prediction much better than grey GM(1,1) model and RBF neural network model.

Keywords: Gas emission prediction; grey theory; RBF neural network model; improved grey RBF neural network model

Preprints (www.preprints.org) | NOT PEER-REVIEWED | Posted: 29 October 2020 doi:10.20944/preprints202010.0613.v1

1. Introduction

Through the years， coal mines have played a crucial role in energy resource around the world. Ranking the first in coal production, China is the largest consumer of coal all over the world which consumed roughly half of the world's coal consumption. Coal exploitation has made an important contribution to development economy in China covering providing employment opportunities and generating purchasing power. Coal still play a dominant role in the total primary energy even though the coal production declined in China [1,2]. Nevertheless, the production system in underground coal mine is a peculiarly complex disaster system ,which caused coal mine accidents occurring frequently [3].

Safe production of underground coal mines is threatened in the extreme by a wide variety of coal mine disaster. In China, high rate accident resulting from coal mine cause huge losses to Chinese economy and thousands of fatalities among coal miners, every year [4].Among various types of coal mine accident, gas accident is normally perceived as the hazardous one [5]. After CO_2, methane is the second-biggest source of global greenhouse gas emission and a major source of methane emission is coal mine [6–8].

Studies have shown that methane emission relevant to coal-mine ventilation has an adverse impact of environment. And methane as a precious clean resources released into the atmosphere is a waste [9,10]. Methane emission from ventilation system is the primary source of coal mine methane emission. In China, there are approximately 85–90% of coal mine methane sourcing from underground coal mine [11].

In addition, methane is an explosive gas which has extremely energy [12]. Therefore, taking advantage of drained methane from coal mine will become critical in lessening methane emission in the atmosphere [13].

In China, coal and gas outburst is the severest cause which are leading to hazard of coal mines, which can let out plenty of coal gas as quick as thought and induce gas explosion. Intense and sudden release of coal and gas from coal mine has given rise to equipment damage and casualties [14–16].

Figure 1 is based on the web of state administration of coal mine safety, which publishes the number of accidents of Chinese situation of coal and gas outburst from 2006 to 2015[17].

Since 1950, extremely serious gas explosion disasters are occurred in China frequently, till 2015 the happening of extremely serious gas explosion disasters having been reaching up to 126 [18]. Hence, it is imminently necessary to carry through an investigation which can accurately prophesy gas outburst, and furnish direction arrangement of tunnel support in coal mine.

Preprints (www.preprints.org) | NOT PEER-REVIEWED | Posted: 29 October 2020 doi:10.20944/preprints202010.0613.v1

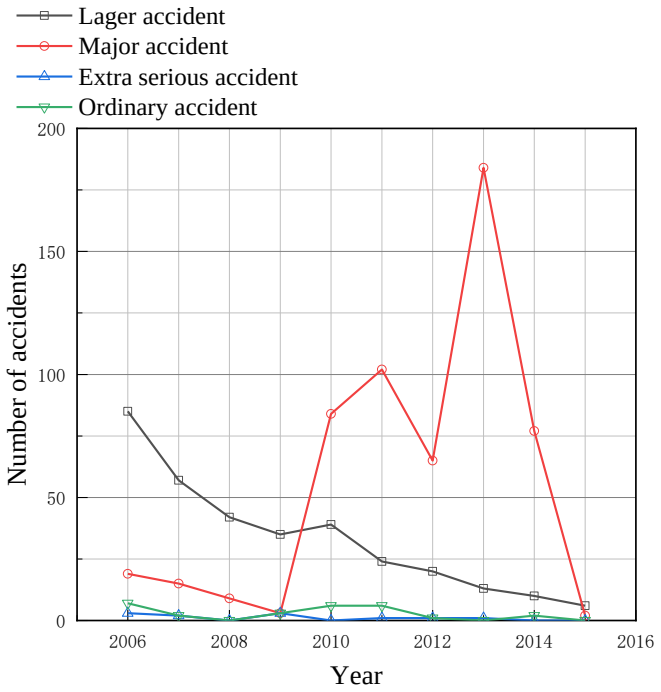

Fig.1 Chinese situation of coal and gas outburst from 2006 to 2015

The energy contained in methane is in direct proportion to its risk degree. For this reason, it is becoming more popular in energy sector [19]. Indeed, abundant methane released during mining may create security problems, but coal mine enterprises can also obtain obvious economic benefits if they use coal mine methane rationally [20]. On account of low concentration of methane, some researchers focused on technologies of treating and recovering methane effectively [21].Meanwhile, in contrast to traditional fossil fuel energy, methane is a cleaner energy resource.

China as the largest coal producer all over the world, in excess of 95% the national coal production from underground coal mine. And comparing surface mines, underground coal mines have higher gas emissions. Enormous amount of methane is released during the mine process, especially from state-owned coal mines which have high-gas content. An estimated amount of 19 billion of cubic meters of methane discharged from China's coal mine every year, leading the world but a few pockets of methane was utilized [11,22–25].

Methane is categorized as an important greenhouse gas. Extracting methane effectively is beneficial to protect the atmosphere [26]. But reality dictates that, in the process of mining, a considerable number of coal mine gas discharged into atmosphere through the ventilation system and a part of unused extracted methane is also released [9]. This may lead global warming and energy waste. Previous research has shown that gas concentration exceeding limit is commonly triggered by high gas emission. And gas concentration transfinite is associated with many serious conditions such as ignition and explosion [27]. Coal mine accidents arising from gas is extremely dangerous and with the increase of depth of the exploited seam, the content of gas increases. Gas emission prediction is crucial to impose restrictions on gas concentration transfinite [28].

In spite of methane consisting in nearly all coal mines in China, it is unrealistic to use other energy in lieu of coal mine in recent years. Mining excavations not only affect economic development, but is also inseparable from the people's livelihood. According to statistics, coal account for 70% of gross energy supply in China [29]. To guarantee the regular national economy, declining the gas emission and improving the utility ratio of extracted methane are appropriate.

Preprints (www.preprints.org) | NOT PEER-REVIEWED | Posted: 29 October 2020 doi:10.20944/preprints202010.0613.v1

Gas emission is admittedly considered as a significant parameter of gas accidents, and has dramatically impacted mining process and the mine ventilation design [30].Hence, to achieve safety production, it is necessary to analysis data in terms of gas emission and forecast its change tendency in advance.

For the sake of processing complex and enormous data connected with gas emission, various forecasting approaches are proposed. The computational fluid dynamic(CFD) was used to simulate methane emission in underground coal mine [31].

As early as the 1996s, researchers have put forward methods to forecast gas emission associated with disturbed and undisturbed longwall faces [32].

With the rapid development of computer technology, in recent years, the numerical simulations were widely used to predict the gas emission.

In order to predicting gas emission quantity precisely, time series analysis on the strength of the Gaussian process regression model was used to gas emission prediction [33]. In study [34], directing at the steeply inclined and extremely thick coal seams, a new method which employed numerical simulation was applied to forecasting gas emission quantity. The issue related gas emission in multifarious geospatial context was analyzed by [35].

Some researchers used several kinds of mathematical models to predict and analyze gas emission simultaneously. Wei et al. focused on the gas emission prediction which based on grey prediction model, new information model as well as metabolism model and compared the results of the three prediction models [36]. Jing et al. used model GM(1,1) of grey and one element linear regression forecasting gas emission simultaneously and conclusions showed that the former has greater precision by contrast [30].

In this study, one improved RBF neutral network model of gas emissions from underground coal mine of China's Shanxi Province is applied to forecast. The analysis included six main affecting factors of gas emissions (coal seam thickness, coal seam spacing, coal seam depth, coal seam gas content, daily production, and daily progress). Processing these factors, a tool used in prediction which associate with gas emission model was built by the artificial neural network. Predictions of gas emission were appeared in this paper and the prediction accuracy was also discussed. Moreover, the paper compared predicted values with actual values.

2. Methods

2.1 RBF neural network

RBF neural network is a model based on Cover which can use primary function approximating arbitrary function.

$$y_i = \sum_{i=1}^{N} w_{ij}\, \phi(\|X - c_i\|),\ i = 1,2,\dots,N \qquad (1)$$

where $X = (x_1, x_2, \dots, x_n)^T \in R^n$, y_i and i represent input vector, output vector and NO. i node, respectively.c_i is the centre and i express NO. i primary function. w_{ij} represent weight between hidden layer and output layer and i as well as j express NO. i of hidden layer and NO. j node of output layer.$\|\cdot\|$ is Euclidean norm. N is the number of centers and hidden layer node. $\phi(\cdot)$ is primary function of hidden layer.

To solve output vector y_i , parameters in the Eq. (1) should be confirmed which are c_i , w_{ij} and $\phi(\cdot)$.

Preprints (www.preprints.org) | NOT PEER-REVIEWED | Posted: 29 October 2020 doi:10.20944/preprints202010.0613.v1

The center c_i of RBF neural network can be determined by means of K-means algorithm. It is considering that elect center can simplify network. Thus, the data which is selected as RBF neural network center should reduce number of element in hidden layer immensely.

Confirming radius δ_i should guarantee the space of training sample that can be contained by the set of acceptance region of RBF unit. The general method for determining c_i and δ_i is employing K-means algorithm, as shown in Eq. (2).

$$\delta_j = \frac{1}{N_j}\sum_{x\in\Gamma_i}(x-c_i)^T(x-c_i) \tag{2}$$

Then using linear least square method adjust weight w_{ij}between the hidden layer and output layer through Eq. (3-4).

$$\mathrm{Y} = \mathrm{W}\cdot\Phi = \mathrm{T} \tag{3}$$

$$\mathrm{W} = \mathrm{T}\Phi^T(\Phi^T\Phi)^{-1} \tag{4}$$

It is a common practice to consider Gaussian function as $\phi(\cdot)$, as shown in Eq. (5).

$$\mathrm{R}(\mathrm{X}-c_i) = \exp\left(-\frac{1}{2\sigma_i^2}\|X-c_i\|^2\right), \qquad i = 1,2,\dots,N \tag{5}$$

where $\mathrm{X} = (x_1, x_2, \dots, x_n)^T$ represent input vector and σ_i is NO. i perceptive variate which defines width. In this equation c_i express center and subscript i represent NO.i primary function. N is the number of nodes in hidden layer.

Eventually, the output vector can be ciphered out though Eq. (6)

$$y_i = \sum_{i=1}^{N} w_{ij}\exp\left(-\frac{1}{2\sigma_i^2}\|X-c_i\|^2\right), \quad i = 1,2,\dots,N \tag{6}$$

2.2 Grey prediction model

The grey prediction model is to process the seemingly irregular data column into a regular data column through a certain method. Therefore, the grey prediction model is to generate a new sequence and also to generate a sequence model.

Modified grey forecasting model GM(1,1) is a valid model of bating randomness of sample data and enhancing accuracy in forecasting gas emission quantity. The first step is to acquire data of factors that can influence gas emission quantity.

By means of computing logarithmic[10] is an eminent way to make data more smoother, for improving accuracy of prediction. The algorithm is shown as below. There are x groups training samples and y groups predicted samples, compute logarithmic of these x+y groups of samples. Take gas emission quantity $Q^{(0)}$ for example:

$$x^{(0)}lnQ^{(0)}(t)(t = 1,2\dots n) \tag{7}$$

Then obtaining x+y groups samples respectively are $x^{(0)}(1), x^{(0)}(2), \dots x^{(0)}(6), x^{(0)}(7)$. Among these samples, $x^{(0)}(1), x^{(0)}(2), \dots x^{(0)}(6)$ correspond six influence factors about gas emission quantity including thickness of coal seam, interval of coal seam, depth of coal seam, concentration of coal seam, daily output, daily progress. And gas emission quantity homologous sample is $x^{(0)}(7)$.

Preprints (www.preprints.org) | NOT PEER-REVIEWED | Posted: 29 October 2020 doi:10.20944/preprints202010.0613.v1

Secondly, a grey predicted model will be built. As the purpose for the model is dealing the stochastic data and making them regular. The most familiar method to establish grey system model is accumulation.

$$x^{(1)}(k) = \sum_{i=1}^{k} x^{(0)}(i) \tag{8}$$

Adding up x groups of training samples receive a list of data:$x^{(1)}(1), x^{(1)}(2), \ldots x^{(1)}(6)$. Then taking these data as a input vector of modified RBF neural network model.

Using grey forecasting model GM(1,1) dispose $x^{(1)}(1), x^{(1)}(2), \ldots x^{(1)}(6)$ series. Firstly, building a differential equation

$$\frac{dx^{(1)}(i)}{dt} + ax^{(1)}(i) = u \ (i = 1,2 \ldots 6) \tag{9}$$

To solve parameters in this equation utilize least square method:

$$\bar{\hat{a}} = \begin{pmatrix} a \\ u \end{pmatrix} = (B^T \cdot B)^{-1} \cdot B^T \cdot y_n \tag{10}$$

Where B and y_n are built by $x^{(1)}(1), x^{(1)}(2), \ldots x^{(1)}(6)$ and $x^{(0)}(1), x^{(0)}(2), \ldots x^{(0)}(6)$ severally.

$$B = \begin{pmatrix} -0.5\left(x^{(1)}(1) + x^{(1)}(2)\right) & 1 \\ -0.5\left(x^{(1)}(2) + x^{(1)}(3)\right) & 1 \\ M & M \\ -0.5\left(x^{(1)}(n-1) + x^{(1)}(n)\right) & 1 \end{pmatrix} \tag{11}$$

$$y_n = \begin{pmatrix} x^{(0)}(2) \\ x^{(0)}(3) \\ M \\ x^{(0)}(n) \end{pmatrix} \tag{12}$$

Finally, to obtain $\hat{x}^{(1)}(6), \hat{x}^{(1)}(7)$,the objective vector of modified RBF neural network model, establish GM(1,1) model :

$$\hat{x}^{(1)}(k+1) = \left(x^{(0)}(1) - \frac{u}{a}\right) \cdot e^{-ak} + \frac{u}{a} \tag{13}$$

The calculated objective vector and input vector were then input to the modified network model for training.

2.2 Modified RBF neural network

Improved RBF Neural Network Structure is shown in Fig.1.

(1) To determine δ the width of the Gaussian function, set a variable A(l), store the sum of heterogeneous outputs, and set a variable B(l) to count the heterogeneous samples, where l, the number of classes is represented.

(2) With (x^1, y^1) as the first sequence, a network is established, and there is only one hidden neuron node in the network. Let $c_1 = x^1$, $A(1) = y^1$, $B(1) = 1$, c_1 is the center of the hidden layer node, and the weight of the hidden layer node to the output

Preprints (www.preprints.org) | NOT PEER-REVIEWED | Posted: 29 October 2020 doi:10.20944/preprints202010.0613.v1

layer is: $w_1 = A(1)/B(1)$.

(3) For the second sequence (x^2, y^2), calculate the distance between x^2 and c_1: $\|x^2 - c_1\|$. If $\|x^2 - c_1\| \le \delta$, then c_1 is the nearest neighbor clustering of x^2, and let $A(1) = A(1) + y^2$, $B(1) = 1$, $w_1 = A(1)/B(1)$;If $\|x^2 - c_1\| > \delta$, let $c_2 = x^2$, $A(2) = y^2$, $B(2) = 1$. c_2 is the hidden node center. A neuron node is added to the hidden layer of step (2), and the weight from the node to the output layer is $w_2 = A(2)/B(2)$.

(4) The k sequence: (x^k, y^k), $k = 3, 4, \cdots, P$, the number of nodes in the hidden layer of the network is M, in which the center of the node is $c_1, c_2, \cdots, c_M$ in order, and the distance between x^k and $c_1, c_2, \cdots, c_M$ is calculated in turn $\|x^k - c_i\|$, $i = 1, 2, \cdots, M$. Let $\|x^k - c_j\| = \min\{\|x^k - c_i\|\}, i = 1, 2, \cdots, M$.

If $\|x^k - c_j\| \le \delta$, then c_j is the nearest-neighbor clustering of x^k, let $A(j) = A(j) + y^k$, $B(j) = B(j) + 1$, $w_j = A(j)/B(j)$, and then $i \ne j$, let $A(i)$, $B(i)$ remain unchanged, $i = 1, 2, \cdots, M$;

If $\|x^k - c_j\| > \delta$, let $c_{M+1} = x^k$, $A(M+1) = y^k$, $B(M+1) = 1$ and let: when $i = 1, 2, \cdots, M$, $A(i)$, $B(i)$ remain unchanged, add a node to the existing hidden layer of the network, the weight of this node to the output layer: $w_{M+1} = A(M+1)/B(M+1)$. Repeat the above steps until the sample classification is completed.

(5) Initialize μ and θ. Where μ is the input layer to output layer weight, θ is the output layer offset, and is a random number in the range [0,1].

(6) Add incentives $x^k = \left[x_0^k, x_1^k, \cdots, x_{n-1}^k\right]$, x_j^k as the input of node j at time k.

(7) Calculation output.

Let the output of the i node of the hidden layer be:

$$R_i(x^k) = \exp(-\|x^k - c_i\|^2 / \delta^2) \tag{14}$$

Preprints (www.preprints.org) | NOT PEER-REVIEWED | Posted: 29 October 2020 doi:10.20944/preprints202010.0613.v1

The network output is:

$$f(x^k)=\sum_{i=1}^{H} w_i R_i(x^k)+\sum_{j=1}^{n}\mu_j x_j^k+\theta \tag{15}$$

(8) Adjustment weight.

The objective function is:

$$E=\frac{1}{2}\sum_k \left\|y^k-f(x^k)\right\|^2 \tag{16}$$

Adjust the weights w, μ, and θ to obtain the increment factor by the gradient descent method, where:

$$\Delta w_j^k=\eta d R_i(x^k) \tag{17}$$

$$\Delta \mu_j^k=\eta d x_j^k \tag{18}$$

$$\Delta \theta^K=\eta d \tag{19}$$

The iteration formula to get weights and biases is:

$$w_i^{k+1}=w_i^k+\Delta w_i^k+\alpha\Delta w_i^{k-1} \tag{20}$$

$$\mu_j^{k+1}=\mu_j^k+\Delta \mu_j^k+\alpha\Delta \mu_j^{k-1} \tag{21}$$

$$\theta^{k+1}=\theta^k+\Delta\theta^k+\alpha\Delta\theta^{k-1} \tag{22}$$

Among them:

$$\mu=\begin{bmatrix}\mu_{11}\ \mu_{12}\cdots\ \mu_{1n}\\ \mu_{21}\ \mu_{22}\cdots\ \mu_{2n}\\ \cdots\ \ \cdots\ \ \cdots\ \ \cdots\\ \mu_{m1}\ \mu_{m2}\cdots\ \mu_{mn}\end{bmatrix} \tag{23}$$

$$w=\begin{bmatrix}w_{11}\ w_{12}\cdots\ w_{1n}\\ w_{21}\ w_{22}\cdots\ w_{2n}\\ \cdots\ \ \cdots\ \ \cdots\ \ \cdots\\ w_{m1}\ w_{m2}\cdots\ w_{mn}\end{bmatrix} \tag{24}$$

$\theta=[\theta_1,\theta_2\cdots,\theta_m]^T$, hidden layer output $R=[R_1,R_2,\cdots,R_H]^T$, w_i represents column i of w, μ_j represents column j of μ, $d=y^k-f(x^k)$, n, H, m in turn indicate the number of input layer, hidden layer and output layer nodes, η represents the learning rate, $0<\eta<1$; α is the momentum factor and $0<\alpha<1$;

Preprints (www.preprints.org) | NOT PEER-REVIEWED | Posted: 29 October 2020 doi:10.20944/preprints202010.0613.v1

k is the number of iterations.

(8) Go to the next sample and repeat steps (6) to (9) until the error $E=\frac{1}{2}\sum_{k}\left\|y^{k}-f(x^{k})\right\|^{2}$ reaches the specified accuracy.

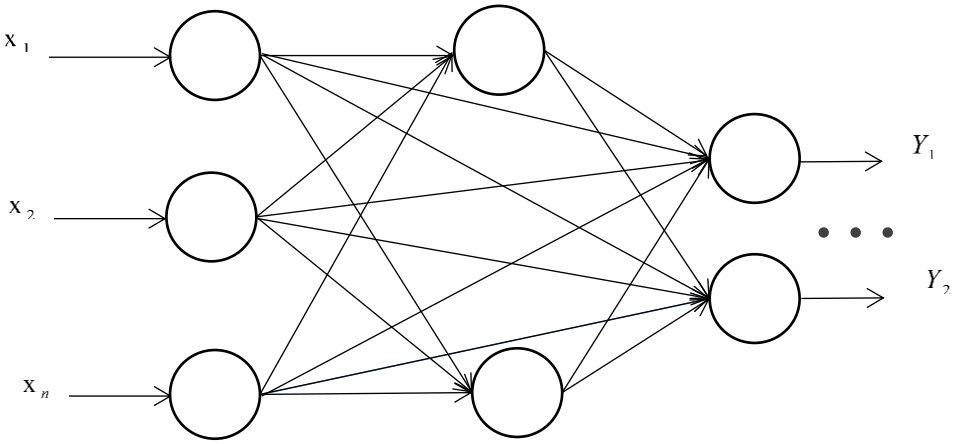

Fig.1 Improved RBF Neural Network Structure

2.3 Modeling and prediction of improved grey RBF neural network model

The modeling and prediction steps of the improved grey RBF neural network model are as follows:

(1) Group x is the training sample and group y is the prediction sample. Obtaining $x^{(0)}(1),x^{(0)}(2),\cdots,x^{(0)}(6),x^{(0)}(7)$ by evaluating the logarithm of the sample x+y, where $x^{(0)}(7)$ in the y group is not processed, $x^{(0)}(1),x^{(0)}(2),\cdots,x^{(0)}(6)$ respectively correspond to the six main factors affecting the gas emission amount, and $x^{(0)}(7)$ corresponds to the gas emission amount;

(2) The x group of training samples $x^{(0)}(1),x^{(0)}(2),\cdots,x^{(0)}(6)$ is accumulated once to obtain $x^{(1)}(1),x^{(1)}(2),\cdots,x^{(1)}(6)$, this data is listed as the input vector of the improved RBF neural network model;

(3) The data column $x^{(0)}(1),x^{(0)}(2),\cdots,x^{(0)}(6),x^{(0)}(7)$ is predicted by the GM (1,1) model to obtain $\overline{\hat{x}}^{(1)}(6)$, $\overline{\hat{x}}^{(1)}(7)$, and $\overline{\hat{x}}^{(1)}(6)$, $\overline{\hat{x}}^{(1)}(7)$ as the target vector;

(4) Input the input vector and target vector in (2) and (3) into the improved RBF neural network training;

(5) The y group of prediction samples $x^{(0)}(1),x^{(0)}(2),\cdots,x^{(0)}(6)$ is accumulated once to obtain $x^{(1)}(1),x^{(1)}(2),\cdots,x^{(1)}(6)$;

Preprints (www.preprints.org) | NOT PEER-REVIEWED | Posted: 29 October 2020 doi:10.20944/preprints202010.0613.v1

(6) Input $x^{(1)}(1), x^{(1)}(2), \cdots, x^{(1)}(6)$ obtained in step (5) into the improved RBF neural network trained in step (4), and obtain predicted values $\bar{\hat{x}}^{(1)}(6)$, $\bar{\hat{x}}^{(1)}(7)$;

(7) Find the difference: $\bar{\hat{x}}^{(0)}(7) = \bar{\hat{x}}^{(1)}(7) - \bar{\hat{x}}^{(1)}(6)$;

(8) Index reduction: $\bar{\hat{Q}}^{(0)}(t) = e^{\bar{\hat{x}}^{(0)}(7)}$, $\bar{\hat{Q}}^{(0)}(t)$ is the final predicted value of gas emission.

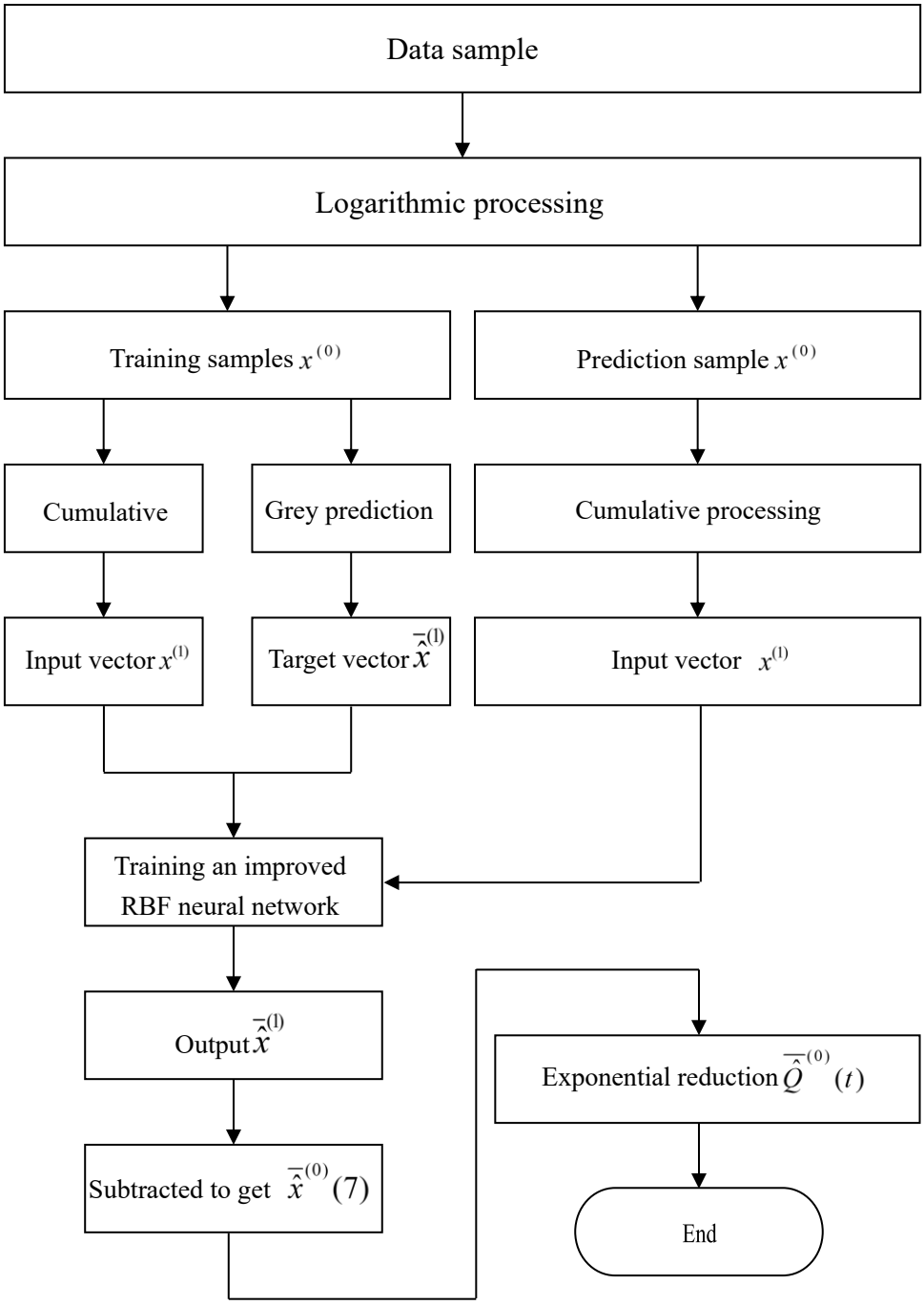

Fig.2 Improved Grey RBF Neural Network Modeling and Prediction Process

Preprints (www.preprints.org) | NOT PEER-REVIEWED | Posted: 29 October 2020 doi:10.20944/preprints202010.0613.v1

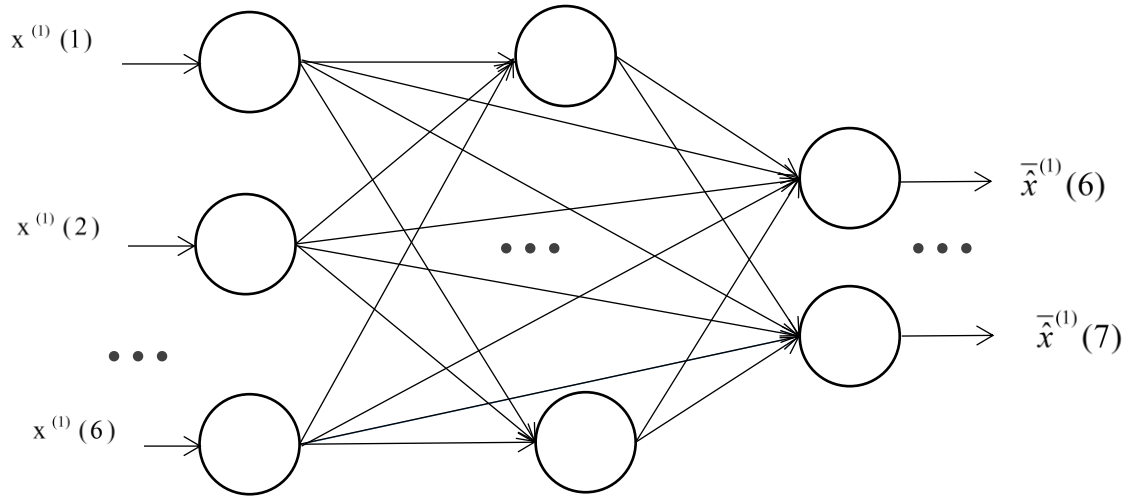

Fig.3 Improved Grey RBF Neural Network Structure Diagram

3. Results and Discussion

In order to test the prediction effect of the model, this paper uses 300 sets of gas data from a coal mine in Shanxi as shown in Table 1. Among them, $x_1, x_2, x_3, x_4, x_5, x_6, x_7$, respectively, represent the coal seam depth, coal seam thickness, coal seam gas content, coal seam spacing, daily progress, daily output, and gas emission. As mentioned in the previous chapters, these six factors are the main influencing factors based on the research results of previous researchers. Therefore, this article will no longer find the main factors through some methods.

The first 275 groups of 1 to 275 groups are taken as training samples, and the last 25 groups of 276 to 300 groups are used as prediction samples to check the prediction accuracy. Using MATLAB 7.8, write programs to build RBF neural network models, grey RBF neural network models, and improved grey RBF neural network models. These three models are used to make predictions respectively. The predicted values are compared with the actual values, and the relative errors of the three models are calculated for analysis and comparison.

Table 1 Gas Sample Data

Sample Serial number	x_1 /(m)	x_2 /(m)	x_3 /(m^3/l)	x_4 /(m)	x_5 /(m/d)	x_6 /(t/d)	x_7 /(m^3/min)
1	312	3.0	2.12	12	3.28	2456	4.12

Preprints (www.preprints.org) | NOT PEER-REVIEWED | Posted: 29 October 2020 doi:10.20944/preprints202010.0613.v1

2	318	3.3	2.22	21	3.24	2784	2.95
3	327	2.7	1.83	17	4.21	2649	3.74
4	356	4.2	3.11	14	4.22	3571	3.86
5	421	2.4	2.34	25	4.13	2974	4.15
6	458	2.1	4.52	14	3.35	3164	4.43
7	489	5.8	3.83	19	3.33	2486	3.78
8	522	2.6	1.92	16	3.41	1987	5.25
9	545	4.1	4.13	23	2.87	2652	6.65
10	589	4.4	4.21	24	2.86	2876	7.47
11	473	3.8	3.37	22	2.58	3087	5.79
12	426	4.3	3.59	21	4.15	2185	3.49
13	487	3.8	2.14	15	3.37	3275	4.98
14	534	4.7	4.19	18	3.93	3347	3.73
15	476	4.2	4.02	23	4.01	3327	4.39

3.1 RBF neural network model prediction

The input vector of the RBF neural network model is the six main factors affecting the gas emission amount, and the output vector is the gas emission amount. The modeling and prediction steps are as follows:

(1) Take the first 275 sets of training samples $x_1, x_2, x_3, x_4, x_5, x_6$ as the input vector and x_7 as the target vector;

(2) Input the input vector and the target vector into the RBF neural network model to learn and train;

Preprints (www.preprints.org) | NOT PEER-REVIEWED | Posted: 29 October 2020 doi:10.20944/preprints202010.0613.v1

(3) The last 25 sets of prediction samples $x_1, x_2, x_3, x_4, x_5, x_6$ are input into the trained RBF neural network model, and the prediction value is calculated;

(4) Finally, we can calculate the relative error.

Figure 4 is the comparison between the predicted and actual values of the model, and Figure 5 is the relative error of the model.

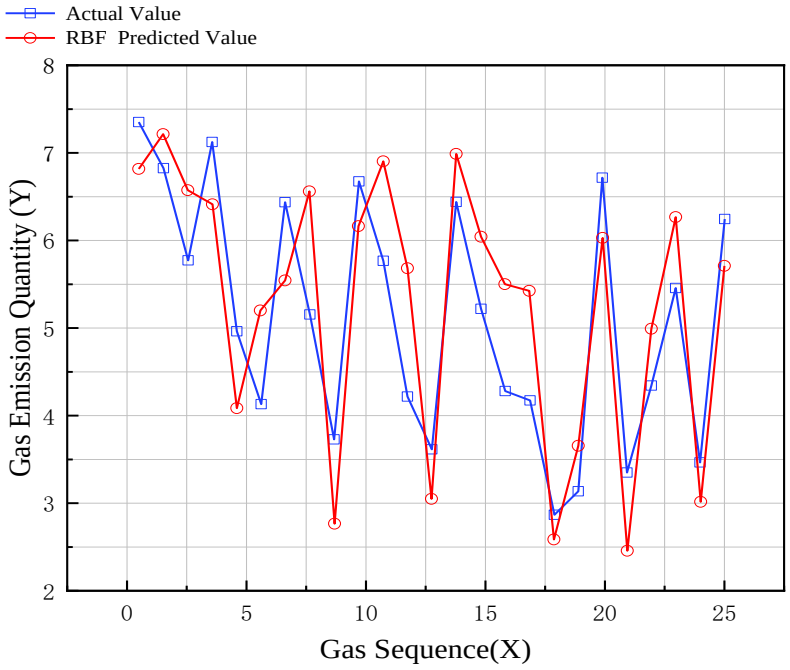

Fig.4 Comparison between RBF Neural Network Model Predicted Value and Actual Value

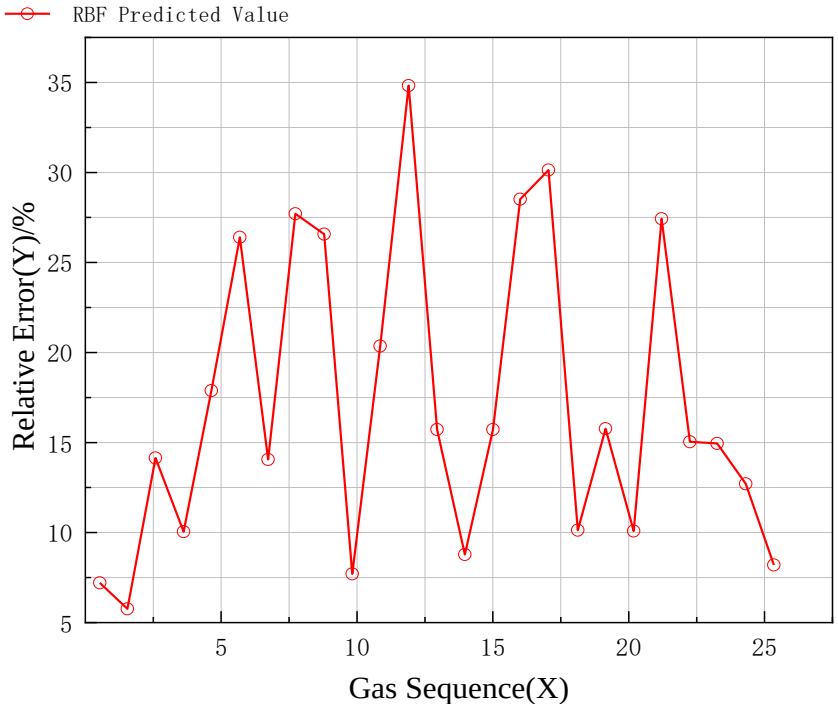

Fig.5 RBF Neural Network Model Relative Error

Preprints (www.preprints.org) | NOT PEER-REVIEWED | Posted: 29 October 2020 doi:10.20944/preprints202010.0613.v1

3.2 Grey RBF neural network model prediction

The grey RBF neural network model combines the GM (1,1) model with the RBF neural network model. The input layer and the output layer are six and two neuron nodes, respectively. The modeling and prediction steps are as follows:

(1) The first 275 sets of training samples $x_1, x_2, x_3, x_4, x_5, x_6$ accumulate to generate a sequence $x^{(1)}(1), x^{(1)}(2),..., x^{(1)}(6)$, which is used as the input vector of the RBF neural network model;

(2) The first 275 sets of training samples $x_1, x_2, x_3, x_4, x_5, x_6, x_7$ are calculated using the GM (1,1) model to obtain $\bar{\hat{x}}^{(1)}(6), \bar{\hat{x}}^{(1)}(7)$,and use $\bar{\hat{x}}^{(1)}(6), \bar{\hat{x}}^{(1)}(7)$ as the target vectors of the RBF neural network model;

(3) Input the input vector and the target vector into the RBF neural network model to learn and train;

(4) A cumulative operation of the last 25 sets of prediction samples $x_1, x_2, x_3, x_4, x_5, x_6$ to obtain the generated sequence;

(5) The generated sequence in (4) is input into the RBF neural network model that has been trained, and the output values are: $\bar{\hat{x}}^{(1)}(6), \bar{\hat{x}}^{(1)}(7)$;

(6) Subtraction: $\bar{\hat{x}}^{(0)}(7) = \bar{\hat{x}}^{(1)}(7) - \bar{\hat{x}}^{(1)}(6)$, $\bar{\hat{x}}^{(0)}(7)$ is the final predicted value;

(7) Find the relative error.

Figure 6 is the comparison between the predicted value and the actual value of the grey RBF neural network model, and Figure 7 is the relative error of the model.

Preprints (www.preprints.org) | NOT PEER-REVIEWED | Posted: 29 October 2020 doi:10.20944/preprints202010.0613.v1

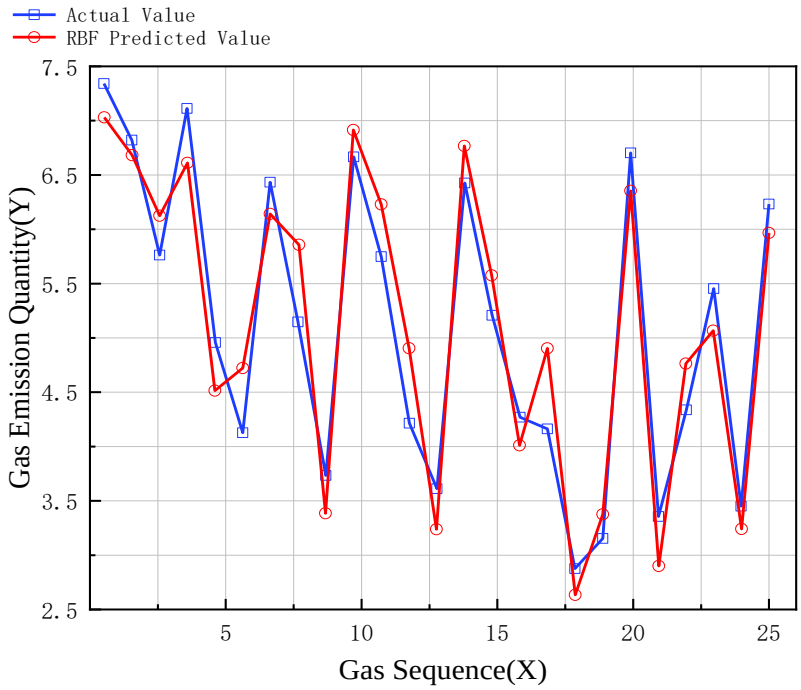

Fig.6 Comparison between Grey RBF Neural Network Model Predicted Value and Actual Value

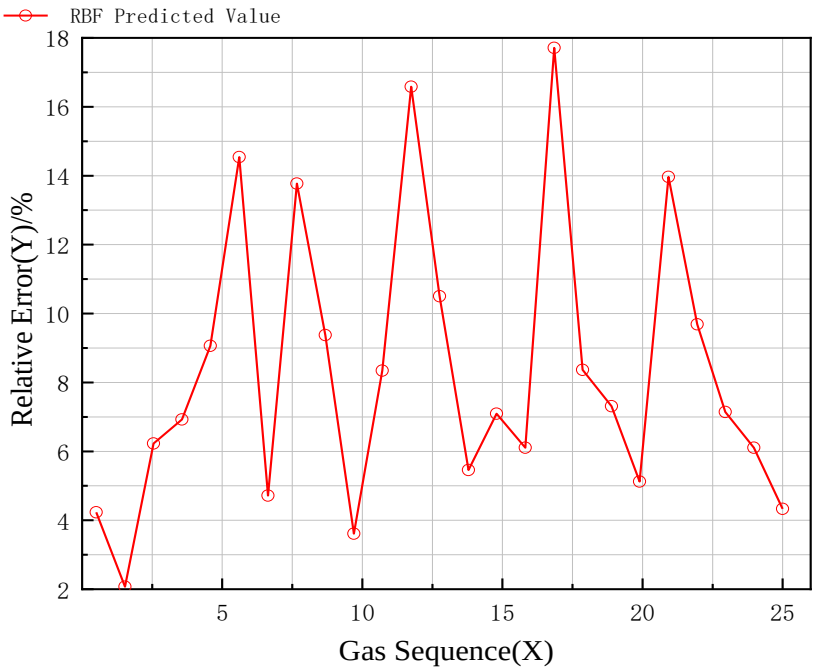

Fig.7 Grey RBF Neural Network Model Relative Error

Preprints (www.preprints.org) | NOT PEER-REVIEWED | Posted: 29 October 2020 doi:10.20944/preprints202010.0613.v1

3. 3 Improved grey RBF neural network model prediction

Follow the steps to build an improved grey RBF neural network model and make predictions. The modeling and prediction steps are as follows:

(1) The first 275 groups of training samples $x_1, x_2, x_3, x_4, x_5, x_6, x_7$ are log processed to obtain the corresponding number series $x^{(0)}(1), x^{(0)}(2),..., x^{(0)}(6), x^{(0)}(7)$. Logarithmic processing of the last 25 groups of prediction samples $x_1, x_2, x_3, x_4, x_5, x_6$ yields $x^{(0)}(1), x^{(0)}(2),..., x^{(0)}(6)$, where x_7 of the last 25 groups does not perform logarithmic processing;

(2) The $x^{(0)}(1), x^{(0)}(2),..., x^{(0)}(6)$ sequence obtained by the first 275 logarithmic processing in (1) is used to accumulate a generated sequence $x^{(1)}(1), x^{(1)}(2), \cdots, x^{(1)}(6)$, which is used as the input vector of the improved RBF neural network model;

(3) Then we can bring $x^{(0)}(1), x^{(0)}(2),..., x^{(0)}(6), x^{(0)}(7)$,which is Obtained by logarithmic processing before 275 groups in step (1), into GM(1,1) and calculate $\overline{\hat{x}}^{(1)}(6), \overline{\hat{x}}^{(1)}(7)$. $\overline{\hat{x}}^{(1)}(6), \overline{\hat{x}}^{(1)}(7)$ is the target vector of the improved RBF neural network model;

(4) A cumulative operation is performed on the $x^{(0)}(1), x^{(0)}(2),..., x^{(0)}(6)$ obtained by the last 25 groups of logarithmic processing to obtain a generated sequence $x^{(1)}(1), x^{(1)}(2), \cdots, x^{(1)}(6)$;

(5) Input $x^{(1)}(1), x^{(1)}(2), \cdots, x^{(1)}(6)$ in (5) into the improved RBF neural network model with completed training, and the output value is : $\overline{\hat{x}}^{(1)}(6), \overline{\hat{x}}^{(1)}(7)$;

(6) Subtract: $\overline{\hat{x}}^{(0)}(7) = \overline{\hat{x}}^{(1)}(7) - \overline{\hat{x}}^{(1)}(6)$;

(7) Index reduction: $\overline{\hat{Q}}^{(0)}(t) = e^{\overline{\hat{x}}^{(0)}(7)}$, $\overline{\hat{Q}}^{(0)}(t)$ is the final predicted value;

(8) Finding the relative error.

3.4 Analysis and comparison of prediction results of three models

Compare the relative errors of the above three models, as shown in Figure 8.

As can be seen from Figure 8, the relative errors of the RBF neural network model, the grey RBF neural network model, and the improved grey RBF neural network model become smaller in order, and the model's prediction accuracy improves in turn, indicating the grey GM (1,1) model The introduction of the method weakens the randomness of the sample, which improves the prediction accuracy of the grey RBF neural network model. It also shows that after introducing the improved GM (1,1)

Preprints (www.preprints.org) | NOT PEER-REVIEWED | Posted: 29 October 2020 doi:10.20944/preprints202010.0613.v1

model and the improved RBF neural network model, compared with the grey RBF neural network model, On the one hand, the sample data becomes smoother, which further weakens the sample randomness. On the other hand, the RBF neural network model has been improved, and the model performance has been improved. Therefore, the improved grey RBF neural network model further improves the prediction accuracy. Among the three models, the improved grey RBF neural network model has the highest prediction accuracy. Besides, the relative errors of the improved grey RBF neural network model are mostly within 5%, and the other few are also basically within 10%.

As can be seen from Figure 6 and 7, the relative errors of the RBF neural network model, the grey RBF neural network model, and the improved grey RBF neural network model become smaller in order, and the model's prediction accuracy improves in turn, indicating the grey GM (1,1) model The introduction of the method weakens the randomness of the sample, which improves the prediction accuracy of the grey RBF neural network model. It also shows that after introducing the improved GM (1,1) model and the improved RBF neural network model, compared with the grey RBF neural network model, On the one hand, the sample data becomes smoother, which further weakens the sample randomness. On the other hand, the RBF neural network model has been improved, and the model performance has been improved. Therefore, the improved grey RBF neural network model further improves the prediction accuracy. Among the three models, the improved grey RBF neural network model has the highest prediction accuracy. Besides, the relative errors of the improved grey RBF neural network model are mostly within 5%, and the other few are also basically within 10%.

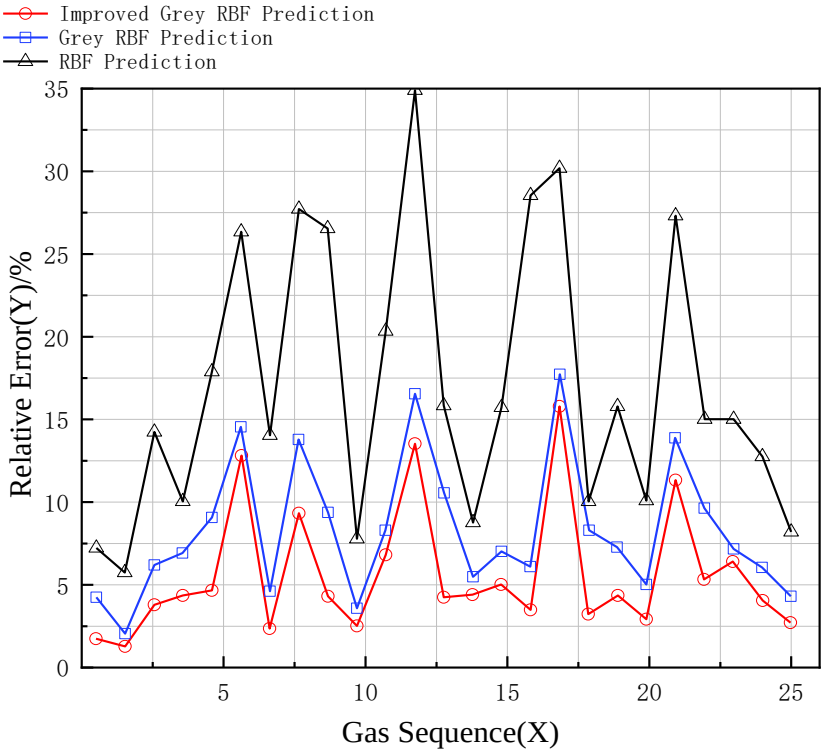

Fig.8 Comparison of Three-model Relative Errors

 doi:10.20944/preprints202010.0613.v1

4. Conclusions

Combining conventional neural network and grey theory, an improved grey RBF neural network model for gas emission prediction is proposed. The main conclusions are as follows:

1. The RBF neural network model has the lowest accuracy, followed by the grey RBF neural network model, and the improved grey RBF neural network model has the highest accuracy. The grey RBF neural network model improves the accuracy of the model by weakening the randomness of the sample. The improved grey RBF neural network model has further improved both in terms of weakening the randomness of sample data and the performance of the network model itself.

2. The relative error of the improved grey RBF neural network model is mostly within 5%, and the other few are basically within 10%, which gives an ideal prediction effect.

Data Availability

The article data used to support the findings of this study are included within the article.

Acknowledgments

This work was supported by the National Natural Science Foundation of China (Grant No. 51404167), Natural Science Foundation of Shanxi Province (Grant No. 201801D121034); Shanxi Provincial Key R&D Project (Grant No. 201803D31051); Shanxi Soft Science Research Project (Grant No. 201803D31051); China postdoctoral science foundation funding project (Grant No. 2016M590151).

References

1. Burgherr, P.; Hirschberg, S. Assessment of severe accident risks in the Chinese coal chain. *International Journal of Risk Assessment & Management* **2007**, *7*, 1157–1175.
2. Geng, F.; Saleh, J.H. Challenging the emerging narrative: Critical examination of coalmining safety in China, and recommendations for tackling mining hazards. *Safety Science* **2015**, *75*, 36–48.
3. Tong, R.; Yang, Y.; Ma, X.; Zhang, Y.; Li, S.; Yang, H. Risk Assessment of Miners' Unsafe Behaviors: A Case Study of Gas Explosion Accidents in Coal Mine, China. *Int. J. Environ. Res. Public Health* **2019**, *16*, 1765.

4. Liu, D.; Xiao, X.; Li, H.; Wang, W. Historical evolution and benefit–cost explanation of periodical fluctuation in coal mine safety supervision: An evolutionary game analysis framework. *European Journal of Operational Research* **2015**, *243*, 974–984.
5. Zhou, X.; Jiang, M.-X. Statistical Analysis and Safety Management on China's Coal Mine Gas Accident from 2006 to 2015. *IETI Transactions on Business and Management Sciences* **2016**, *1*, 29–38.
6. Myhre, G.; Shindell, D.; Bréon, F.-M.; Collins, W.; Fuglestvedt, J.; Huang, J.; Koch, D.; Lamarque, J.-F.; Lee, D.; Mendoza, B.; et al. Anthropogenic and natural radiative forcing. In *Climate Change 2013: The Physical Science Basis. Contribution of Working Group I to the Fifth Assessment Report of the Intergovernmental Panel on Climate Change*; Stocker, T.F., Qin, D., Plattner, G.-K., Tignor, M., Allen, S.K., Doschung, J., Nauels, A., Xia, Y., Bex, V., Midgley, P.M., Eds.; Cambridge University Press: Cambridge, UK, 2013; pp 659–740.
7. Balcombe, P.; Speirs, J.F.; Brandon, N.P.; Hawkes, A.D. Methane emissions: choosing the right climate metric and time horizon. *Environ. Sci.: Processes Impacts* **2018**, *20*, 1323–1339.
8. Daniel J.G. Crow; Paul Balcombe; Nigel Brandon; Adam D. Hawkes. Assessing the impact of future greenhouse gas emissions from natural gas production. *Science of The Total Environment* **2019**, *668*, 1242–1258.
9. Krzysztof Warmuzinski. Harnessing methane emissions from coal mining. *Process Safety and Environmental Protection* **2008**, *86*, 315–320.
10. Shi, S.; Han, J.; Wu, J.; Li, H.; Worrall, R.; Hua, G.; Xin, S.; Liu, W. Fugitive coal mine methane emissions at five mining areas in China. *Atmospheric Environment* **2011**, *45*, 2220–2232.
11. Cheng, Y.-P.; Wang, L.; Zhang, X.-L. Environmental impact of coal mine methane emissions and responding strategies in China. *International Journal of Greenhouse Gas Control* **2011**, *5*, 157–166.
12. *ANALYSIS OF METHANE EMISSION INTO THE ATMOSPHERE AS A RESULT OF MINING ACTIVITY*. *International Multidisciplinary Scientific Geoconference Sgem;* Tutak, M.; Brodny, J., Eds., 2017.
13. Setiawan, A.; Eric M. Kennedy; Stockenhuber, M. Development of Combustion Technology for Methane Emitted from Coal‐Mine Ventilation Air Systems. *Energy Technology* **2017**, *5*.
14. Sun, H.; Cao, J.; Li, M.; Zhao, X.; Dai, L.; Sun, D.; Wang, B.; Zhai, B. Experimental Research on the Impactive Dynamic Effect of Gas-Pulverized Coal of Coal and Gas Outburst. *Energies* **2018**, *11*.
15. Li, Z.; Wang, E.; Ou, J.; Liu, Z. Hazard evaluation of coal and gas outbursts in a coal-mine roadway based on logistic regression model. *International Journal of Rock Mechanics and Mining Sciences* **2015**, *80*, 185–195.
16. Zhou, H.; Yang, Q.; Cheng, Y.; Ge, C.; Chen, J. Methane drainage and utilization in coal mines with strong coal and gas outburst dangers: A case study in Luling mine, China. *Journal of Natural Gas Science and Engineering* **2014**, *20*, 357–365.
17. National Coal Mine Safety Administration. http://www.chinacoal-safety.gov.cn/gk/sgcc/ (accessed on 1 July 2020).
18. Zhang, J.; David, C.; Xu, K.; You, G. Focusing on the patterns and characteristics of extraordinarily severe gas explosion accidents in Chinese coal mines. *Process Safety &*

Environmental Protection **2018**, *117*, 390–398.

19. Magdalena Tutak; Jarosaw Brodny. Forecasting Methane Emissions from Hard Coal Mines Including the Methane Drainage Process. *Energies* **2019**, *12*, 1–29.
20. Karacan, C.Ö.; Ruiz, F.A.; Cotè, M.; Phipps, S. Coal mine methane: A review of capture and utilization practices with benefits to mining safety and to greenhouse gas reduction. *Int. J. Coal Geol.* **2011**, *86*, 121–156.
21. Yang, X.; Liu, Y.; Li, Z.; Zhang, C.; Xing, Y. Vacuum Exhaust Process in Pilot-Scale Vacuum Pressure Swing Adsorption for Coal Mine Ventilation Air Methane Enrichment. *Energies* **2018**, *11*, 1030.
22. Ju, Y.; Li, X. New research progress on the ultrastructure of tectonically deformed coals. *Progress in Natural Science* **2009**, *19*, 1455–1466.
23. Zhang, B.; Chen, G.Q. Methane emissions by Chinese economy: Inventory and embodiment analysis. *Energy Policy* **2010**, *38*, 4304–4316.
24. Zhang, B.; Chen, G.Q.; Li, J.S.; Tao, L. Methane emissions of energy activities in China 1980–2007. *Renewable and Sustainable Energy Reviews* **2014**, *29*, 11–21.
25. Li, W.; Younger, P.L.; Cheng, Y.; Zhang, B.; Zhou, H.; Liu, Q.; Dai, T.; Kong, S.; Jin, K.; Yang, Q. Addressing the CO 2 emissions of the world's largest coal producer and consumer: Lessons from the Haishiwan Coalfield, China. *Energy* **2015**, *80*, 400–413.
26. Liu, Y.; Wang, F.; Tang, H.; Liang, S. Well type and pattern optimization method based on fine numerical simulation in coal-bed methane reservoir. *Environ Earth Sci* **2015**, *73*, 5877–5890.
27. Guo, P.; Cheng, Y.; Jin, K.; Liu, Y. The impact of faults on the occurrence of coal bed methane in Renlou coal mine, Huaibei coalfield, China. *Journal of Natural Gas Science and Engineering* **2014**, *17*, 151–158.
28. Liu, S.; Xie, L.; Zhang, S. Synchronization of a class of nonlinear network flow systems. *Int. J. Robust. Nonlinear Control* **2016**, *26*, 565–577.
29. He, X.; Song, L. Status and future tasks of coal mining safety in China. *Safety Science* **2012**, *50*, 894–898.
30. Guo-xun, J.; Sheng-ming, X.; Xian-wei, H.; Chuang-qi, L. Research on the Prediction of Gas Emission Quantity in Coal Mine Based on Grey System and Linear Regression for One Element. *Procedia Engineering* **2011**, *26*, 1585–1590.
31. Devi Prasad Mishra; Pradeep Kumar; Durga Charan Panigrahi. Dispersion of methane in tailgate of a retreating longwall mine: a computational fluid dynamics study. *Environ Earth Sci* **2016**, *75*, 1–10.
32. Noack, K. Control of gas emissions in underground coal mines. *Int. J. Coal Geol.* **1998**, *35*, 57–82.
33. Dong, D. Mine Gas Emission Prediction based on Gaussian Process Model. *Procedia Engineering* **2012**, *45*, 334–338.
34. Cheng, L.; Shugang, L.; Shouguo, Y. Gas emission quantity prediction and drainage technology of steeply inclined and extremely thick coal seams. *International Journal of Mining Science and Technology* **2018**, *28*, 415–422.
35. Booth, P.; Brown, H.; Nemcik, J.; Ting, R. Spatial context in the calculation of gas emissions for underground coal mines. *International Journal of Mining Science and Technology* **2017**, *27*, 787–794.

 doi:10.20944/preprints202010.0613.v1

36. Chunrong, W.; Minqiang, X.; Jianhua, S.; Xiang, L.; Chenrun, J. Coal Mine Gas Emission Grey Dynamic Prediction. *Procedia Engineering* **2011**, *26*, 1157–1167.